Article

Backbone Dynamics in the DNA *Hha*I Protein Binding Site

Kari Pederson, Gary A. Meints, Zahra Shajani, Paul A. Miller, and Gary P. Drobny

J. Am. Chem. Soc., **2008**, 130 (28), 9072-9079 • DOI: 10.1021/ja801243d • Publication Date (Web): 21 June 2008

J|A|C|S
ARTICLES

Published on Web 06/21/2008

Backbone Dynamics in the DNA *Hha*I Protein Binding Site

Kari Pederson,[†] Gary A. Meints,[‡] Zahra Shajani,[†,§] Paul A. Miller,[†] and Gary P. Drobny*[,†]

Department of Chemistry, University of Washington, Seattle, Washington 98195-1700, and Department of Chemistry, Missouri State University, Springfield, Missouri 65897

Received February 21, 2008; E-mail: drobny@chem.washington.edu

Abstract: The dynamics of the phosphodiester backbone in the [5′-GCGC-3′]$_2$ moiety of the DNA oligomer [d($G_1A_2T_3A_4\underline{G}_5\underline{C}_6\underline{G}_7\underline{C}_8T_9A_{10}T_{11}C_{12}$)]$_2$ are studied using deuterium solid-state NMR (SSNMR). SSNMR spectra obtained from DNAs nonstereospecifically deuterated on the 5′ methylene group of nucleotides within the [5′-GCGC-3′]$_2$ moiety indicated that all of these positions are structurally flexible. Previous work has shown that methylation reduces the amplitude of motion in the phosphodiester backbone and furanose ring of the same DNA, and our observations indicate that methylation perturbs backbone dynamics through not only a loss of mobility but also a change of direction of motion. These NMR data indicate that the [5′-GCGC-3′]$_2$ moiety is dynamic, with the largest amplitude motions occurring nearest the methylation site. The change of orientation of this moiety in DNA upon methylation may make the molecule less amenable to binding to the *Hha*I endonuclease.

1. Introduction

Methylation of nucleotide bases is important for many biological processes[1–5] from embryogenesis[6] to facilitation of B−A and B−Z transitions.[7–10] The *Hha*I system in particular is a restriction−modification system consisting of a methyltransferase (Mtase) and endonuclease, which together act as a defense mechanism in prokaryotic systems, protecting the cell from invasive DNA. Both proteins recognize the sequence [5′-G↓$\underline{C}$GC-3′]$_2$ (the arrow indicates cleavage and the underlined cytosine base is the methylation target). The Mtase DNA target forms a classic B-form double helix, providing no path to methylate the cytidine base; however, the crystal structure of the *Hha*I Mtase-cognate DNA ternary complex, consisting of the Mtase, the cognate DNA, and the *S*-adenosyl-methionine (Ado-Met) cofactor, demonstrates that the cytosine is exohelical and is surrounded in the binding pocket of the Mtase (Figure 1A).[11] The physical removal from the stacked base in the helix explains how the methylation position of the base is accessible; however, it is still unclear whether flipping of the target base occurs through an active (protein-induced) or passive (captured) process. Previously, computational and NMR imino proton exchange studies supported passive flipping;[12,13] however, more

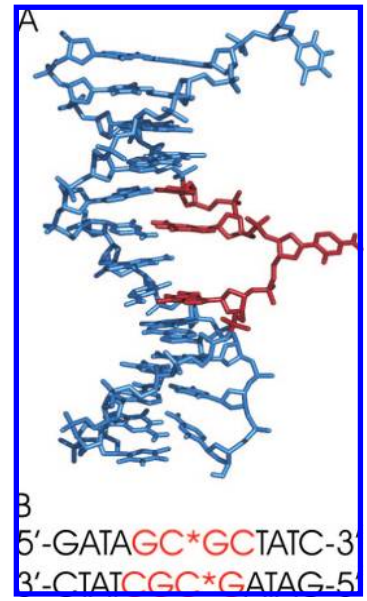

Figure 1. (A) Structure of the *Hha*I target DNA in the protein−DNA complex (protein removed), showing the extrahelical deoxycytidine. The recognition sequence is shown in red. (B) Sequence of the target DNA; residues highlighted in red are both labeled at the 5′/5″ position and part of the recognition sequence.

[†] University of Washington.
[‡] Missouri State University.
[§] Current address: Department of Molecular Biology, The Scripps Research Institute, 10550 North Torrey Pines Road MB-33, La Jolla, CA 92037.

(1) Bird, A. *Cancer Surv.* **1996**, *28*, 87–101.
(2) Jones, P. A.; Baylin, S. B. *Nat. Rev. Genet.* **2002**, *3*, 415–428.
(3) Robertson, K. D. *Nat. Rev. Genet.* **2005**, *6*, 597–610.
(4) Ahmad, I.; Rao, D. *Crit. Rev. Biochem. Mol. Biol.* **1996**, *31*, 361–380.
(5) Chela-Flores, J. *Int. J. Theor. Phys.* **1990**, *29*, 361–380.
(6) Egger, G.; Liang, G.; Aparicio, A.; Jones, P. A. *Nature* **2004**, *429*, 457–463.
(7) Frederick, C. A.; Saal, D.; van der Marel, G.; van Boom, J. H.; Wang, A. H.-J.; Rich, A. *Biopolymers* **1987**, *26*, S145–S160.
(8) Mooers, B. H. M.; Schroth, G. P.; Baxter, W. W.; Ho, P. S. *J. Mol. Biol.* **1995**, *249*, 772–784.
(9) Behe, M.; Felsenfeld, G. *Proc. Natl. Acad. Sci. U.S.A.* **1981**, *78*, 1619–1623.
(10) Fujii, S.; Wang, A. H.-J.; van der Marel, G.; van Boom, J. H.; Rich, A. *Nucleic Acids Res.* **1982**, *10*, 7879–7892.
(11) Klimasauskas, S.; Kumar, S.; Roberts, R. J.; Cheng, X. *Cell* **1994**, *76*, 357–369.

10.1021/ja801243d CCC: $40.75

recent computational and mutational studies give evidence to support active flipping[14–19] through the major groove pathway.[20–22]

Crystal structures of the DNA-*Hha*I Mtase complex, where the target C is altered to A, U, or an abasic site to form a mismatched base-pair demonstrate that base flipping still occurs.[23,24] This strongly suggests that the primary interaction between the protein and the DNA that induces base flipping would have to occur between the protein and the phosphodiester backbone of the DNA. The large-scale conformational changes of the target nucleotide required for interaction with the Mtase imply that it is reasonable to expect that some form of conformational flexibility of the phosphodiester backbone may characterize the native DNA binding site to overcome the energetic barrier required for such torsion angle changes. A computational study by Banavali and co-workers found that the α, β, ε, and ζ torsional angles of the two phosphodiester groups surrounding the target base occupy many different states, supporting a more flexible phosphodiester group.[25]

The recognition process between the Mtase the methylation target has been amply studied;[16,26–30] yet, so far there has been only a limited quantitative analysis of the effect of methylation on the backbone of the target site in this sequence[31,32] and very few studies on the recognition mechanism of the endonuclease.[33] To date, there is no crystal structure of the endonuclease and target DNA. Recent analysis of the motion of the furanose ring by SSNMR of the nucleotides in and around the recognition sequence of the *Hha*I methyltransferase target DNA has shown that the 2′-deoxycytidine (dC) residues in the recognition sequence have only one favored conformation but exhibit a much larger amplitude of motion than the other residues in and around the recognition sequence.[34]

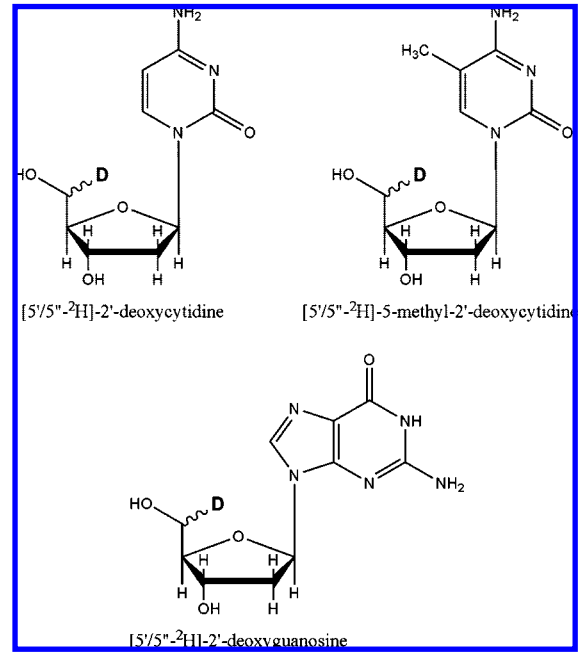

Figure 2. Nonstereospecific labeling of 2′-dC, 2′-dG, and 5-methyl-2′-dC at the 5′/5″ position.

We have previously suggested that motions specific to the *Hha*I target sequence facilitate base extrusion by decreasing energetic barriers. In our present study, we are also interested in quantifying and understanding the degree to which methylation perturbs the local dynamics of the DNA sequence. We have extended our studies to investigate the range of motions of the phosphodiester backbone within the recognition site by reporting SSNMR line shape and relaxation data and to investigate the angular trajectories of these motions by modeling the deuterium solid-state line shapes of the 5′/5″ deuterons in the protein recognition site. We observe increased conformational flexibility in the backbone of the target site, which is "quenched," and the direction of motion is altered, upon methylation, suggesting how dynamics may assist the endonuclease in discerning between methylated and unmethylated DNA.

2. Experimental Methods

2.1. Synthesis. Deuterium labels were incorporated nonstereospecifically into the 5′ methylene group at positions dG5, dC6, dG7, dC8, and 5-methyl-dC6 in $[d(G_1A_2T_3A_4\underline{G_5}\underline{C_6}\underline{G_7}\underline{C_8}T_9A_{10}T_{11}C_{12})]_2$ (Figures 1B and 2). [5′/5″-^{2}H]-2′-dC and [5′/5″-^{2}H]-2′-dG were synthesized by a method similar to that of Orban and Reid.[35] The starting material for the dC synthesis was N^4-3′-*O*-acetyl-2′-dC, which was purchased from Sigma. The starting material for the dG synthesis was N^2-isobutyryl-3′-*O*-acetyl-2′-dG, synthesized from N^2-isobutyryl-5′-(dimethoxytrityl)-2′-dG. The 3′ hydroxyl group was acetylated with acetic anhydride and purified. N^2-isobutyryl-5′-(dimethoxytrityl)-3′-*O*-acetyl-2′-dG was converted to N^2-isobutyryl-3′-*O*-acetyl-2′-dG by deprotection of the 5′-dimethoxytrityl derivative in 0.25 M trichloroacetic acid in chloroform and purified by silica gel chromatography. The starting material for the 5-methyl-

(12) Chen, Y. Z.; Mohan, V.; Griffey, R. H. *Phys. Rev. E* **2000**, *62*, 1133–1137.
(13) Dornberger, U.; Leijon, M.; Fritzsche, H. *J. Biol. Chem.* **1999**, *274*, 6957–6962.
(14) Klimasauskas, S.; Szyperski, T.; Serva, S.; Wüthrich, K. *EMBO J.* **1998**, *17*, 317–324.
(15) Shieh, F.-K.; Youngblood, B.; Reich, N. O. *J. Mol. Biol.* **2006**, *362*, 516–527.
(16) Zhou, H.; Shatz, W.; Purdy, M. M.; Fera, N.; Dahlquist, F. W.; Reich, N. O. *Biochemistry* **2007**, *46*, 7261–7268.
(17) Estabrook, R. A.; Lipson, R.; Hopkins, B.; Reich, N. O. *J. Biol. Chem.* **2004**, *279*, 31419–31428.
(18) Huang, N.; Banavali, N. K.; MacKerell, A. D., Jr *Proc. Natl. Acad. Sci. U.S.A.* **2003**, *100*, 68–73.
(19) Huang, N.; MacKerell, A. D., Jr *Phil. Trans. R. Soc. Lond. A* **2004**, *362*, 1439–1460.
(20) Bouvier, B.; Grubmüller, H. *Biophys. J.* **2007**, *93*, 770–786.
(21) Luo, J.; Bruice, T. C. *Proc. Natl. Acad. Sci. U.S.A.* **2005**, *102*, 16194–16198.
(22) Horton, J. R.; Ratner, G.; Banavali, N. K.; Huang, N.; Choi, Y.; Maier, M. A.; Marquez, V. E.; MacKerell, A. D., Jr.; Cheng, X. *Nucleic Acids Res.* **2004**, *32*, 3877–3886.
(23) Kumar, S.; Horton, J. R.; Jones, G. D.; Walker, R. T.; Roberts, R. J.; Cheng, X. *Nucleic Acids Res.* **1997**, *25*, 2773–2783.
(24) O'Gara, M.; Horton, J. R.; Roberts, R. J.; Cheng, X. *Nat. Struct. Biol.* **1998**, *5*, 872–877.
(25) Banavali, N. K.; Huang, N.; MacKerell, A. D., Jr *J. Phys. Chem. B* **2006**, *110*, 10997–11004.
(26) Cheng, X.; Roberts, R. J. *Nucleic Acids Res.* **2001**, *29*, 3784–3795.
(27) Daujotyte, D.; Serva, S.; Vilkaitis, G.; Merkiene, E.; Venclovas, C.; Klimasauskas, S. *Structure* **2004**, *12*, 1047–1055.
(28) Varnai, P.; Djuranovic, D.; Lavery, R.; Hartmann, B. *Nucleic Acids Res.* **2002**, *30*, 5398–5406.
(29) Youngblood, B.; Buller, F.; Reich, N. O. *Biochemistry* **2006**, *45*, 15563–15572.
(30) Estabrook, R. A.; Reich, N. O. *J. Biol. Chem.* **2006**, *281*, 37205–37214.
(31) Meints, G. A.; Drobny, G. P. *Biochemistry* **2001**, *40*, 12436–12443.
(32) Banyay, M.; Gräslund, A. *J. Mol. Biol.* **2002**, *324*, 667–676.
(33) Vardimon, L.; Rich, A. *Proc. Natl. Acad. Sci. U.S.A.* **1984**, *81*, 3268–3272.
(34) Meints, G. A.; Miller, P. A.; Pederson, K.; Shajani, Z.; Drobny, G. P. *J. Am. Chem. Soc.* **2008**, *130*, 7305–7314.
(35) Orban, J.; Reid, B. R. *J. Labeled Compd. Radiopharmaceuticals* **1989**, *27*, 195–198.

dC synthesis was 3′-*O*-Acetylthymidine, which was oxidized to the aldehyde by the method of Orban and Reid and subsequently treated with trifluoroacetic acid to prevent base-promoted elimination of the acetate group.[35] Sodium borodeuteride reduction of the crude residue, followed by chromatography on silica gel, gave [5′/5″-^{2}H]-dT. Deuterated nucleosides were converted to *N*-acyl-5′-*O*-(dimethoxytrityl)-3′-*O*-(2-cyanoethyl-*N*,*N*-diisopropylphosphoramidite) as described previously,[36] and the thymidine was converted to its N4-triazole derivative using the procedure of Cowart et al.[37] Deprotection of the DNA in concentrated ammonia (2 days, 55 °C) converted the N4-protected thymidine derivative to [5′/5″-^{2}H]-5-methyl-2′-deoxycytidine. Oligonucleotides were purified on Sephadex size exclusion resin, salted (10% NaCl by weight), packed into a 5 mm solid-state NMR Kel-F sample chamber, and hydrated by vapor diffusion in a humidity chamber containing saturated salts in deuterium-depleted water (75% relative humidity at 20 °C).[38] The water content was quantified gravimetrically by the parameter W (number of water molecules per nucleotide base pair) and is accurate to ±1 waters per nucleotide base pair.

2.2. Solid-State NMR Spectroscopy. All experiments were performed on a home-built NMR spectrometer, operating at a deuterium Larmor frequency of 76.776 MHz, corresponding to a magnetic field strength of 11.74 T. A quadrupolar echo pulse sequence with an eight-step phase cycling scheme was implemented with a delay of 40 μs between 90° pulses (typically 2.6 μs in duration) and a dwell time of 200 ns during acquisition. Data acquisition was initiated prior to the echo maximum. The time domain data were left-shifted and apodized with up to 3000 Hz Lorentzian line broadening prior to Fourier transformation (based on signal-to-noise). Typical experimental times were 72−96 h per line shape, or ∼500K+ scans. Partially relaxed line shapes and spin−lattice relaxation times were determined using an inversion recovery pulse sequence, which incorporated a 180° composite pulse to ensure broadband excitation.[39] To obtain powder-averaged Zeeman spin−lattice relaxation times, $\langle T_{1Z} \rangle$, the integrated intensity of the powder spectrum was monitored as a function of recovery time and analyzed using a nonlinear least-squares fitting routine (Figure 6).[40] Variations in signal-to-noise were due to differences in sample size. The relaxation and line shape measurements reported in this study are for DNA samples equilibrated at 75−80% relative humidity, which correspond to hydration levels of $W = 10-11.8$ moles of water per mole of nucleotide base pairs. As mentioned in the section 2.1, the absolute uncertainly in W is ± 1 water per nucleotide base pair or a relative uncertainly of about 9−10% in the range studied. For crystalline DNA in the B form, the hydration level is approximately $W = 10$. Therefore, the relaxation and line shape data presented here are characteristic of a DNA in a B-form helix. In all experimental spectra shown, the line shapes have been symmetrized about the center of the spectrum to remove any artifacts from imperfect pulses; the center isotropic peak is due to residual HDO.

2.3. Simulations. Simulated line shapes were calculated from parameters describing the global and local motions (Figure 3) using the program MXET1 developed by the Vold group.[41] To simulate the deuterium line shape, a form of the potential energy surface/landscape, $U(\phi_i)$, (through which the C−D bond is traversing) must be chosen. A number of simple jump models have been used to simulate deuterium line shape data acquired from the 5′ methylene groups of the phosphodiester backbones of several DNA sequences. Previously, the local motion of the 5′ methylene group has been modeled as a three-site gauche−trans isomerization,[31] as a two-site jump, and as a biaxial four-site jump.[42,43] These simple models have only approximated the experimental line shapes acquired for the 5′ methylene deuterons in DNA.

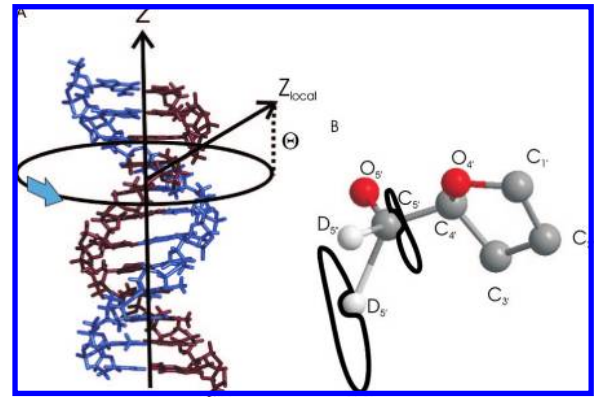

Figure 3. Dynamic axes and coordinate systems used in the studies of backbone dynamics. (A) Line shape simulations include two independent motions. A slow (rate of 10^4 Hz) uniform rotation of the DNA molecule occurs about the helical symmetry axis, labeled Z. Local motion of the backbone is referenced to a local coordinated system, where the z axis is indicated by the vector Z_{local} defined by the angle Θ. (B) Elliptical trajectories for C5′ and D5′/5″.

2.3.1. General Formalism for ^{2}H Line Shape Calculations. Most models proposed to simulate phosphodiester motions in nucleic acids assume segments of the backbone exchange between discrete conformations. Exchanges between discrete structural conformers adequately describe internal molecular reorientations when energy barriers exceed $10k_BT$; however, the barriers between conformational isomers of the phosphodiester backbone are likely much lower than $10k_BT$ so a more realistic model of motion must be invoked. More realistic models of phosphodiester conformational dynamics model the motions of the constituent bonds as Brownian diffusers that move over energy barriers that intervene between low-energy conformers. A great deal of work has been done on the Brownian dynamics of polymethylene chains, mostly in the context amino acid side chain motions in proteins and polymethylene chain motions in lipids.[44] Solutions of the relevant Fokker−Planck equations can be achieved by a discretization scheme as described by Nadler and Schulten.[45] The application of these methods to describing the dynamics of furanose rings has been described in the literature and has succeeded in providing excellent fits to experimental ^{2}H SSNMR line shapes.[31,34] As this formalism has been adequately described in the literature, here we only outline the method briefly.

The experimental ^{2}H SSNMR line shape is fit using the discretization scheme of Nadler and Schulten,[45] which requires construction of an exchange matrix π with elements defined as

$$\begin{aligned} \pi_{ij} &= \frac{1}{\tau}\left(\frac{W_i}{W_{i\pm1}}\right)^{1/2}; j = i \pm 1 \\ \pi_{ij} &= -(\pi_{i,j-1} + \pi_{i,j+1}); j = i \\ \pi_{ij} &= 0; \text{otherwise} \end{aligned} \tag{1}$$

where $W_i = (e^{-U_i/k_BT})Q$, U_i is the value of the potential at the ith discrete site along the reorientational trajectory, and $Q = \sum_i e^{U_i/k_BT}$. The correlation time τ is related to the coefficient of

(36) *Oligonucleotide Synthesis: A Practical Approach*; Gait, M., Ed.; IRL Press: Washington D.C., 1984.
(37) Cowart, M.; Gibson, K. J.; Allen, D. J.; Benkovic, S. J. *Biochemistry* **1989**, *28*, 1975–1983.
(38) Weast, R. C. *CRC Handbook of Chemistry and Physics*; CRC: Boca Raton, FL, 1979.
(39) Tycko, R. *Phys. Rev. Lett.* **1983**, *51*, 775–777.
(40) deFontaine, D.; Ross, D.; Ternai, B. *J. Magn. Reson.* **1975**, *18*, 276–281.
(41) Vold, R. R.; Vold, R. L. *Adv. Magn. Opt. Spectr.* **1991**, *16*, 85–171.
(42) Alam, T. M.; Orban, J.; Drobny, G. P. *Biochemistry* **1991**, *30*, 9229–9237.
(43) Hatcher, M. E.; Mattiello, D. L.; Meints, G. A.; Orban, J.; Drobny, G. P. *Biochemistry* **1998**, *120*, 9850–9862.
(44) Wittebort, R. J.; Olejniczak, E. T.; Griffin, R. G. *J. Chem. Phys.* **1987**, *86*, 5411–5420.
(45) Nadler, W.; Schulten, K. *J. Chem. Phys.* **1986**, *84*, 4015–4025.

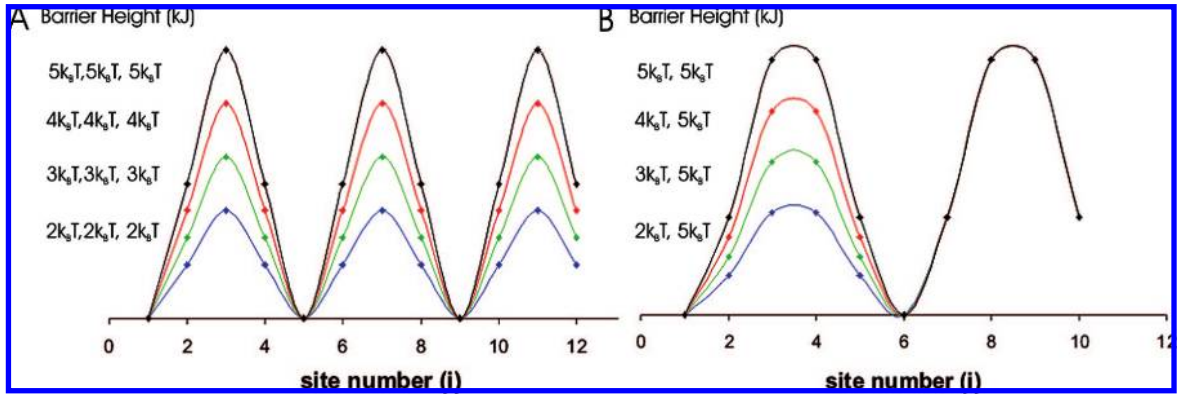

Figure 4. (A) Three-well potential of the form $U(\phi_i) = (U_0/2)(1 - \cos 3\phi_i)$ with varying equal barrier heights. (B) Barrier heights can also be varied throughout the potential as in the two-well potential of the form $U(\phi_i) = (U_0/2)(1 - \cos 2\phi_i)$.

reorientational diffusion D by $\delta^2 = 2D\tau$ where δ is the unit angular displacement.

With the jump matrix constructed according to eq 1, the ^{2}H line shape is obtained as outlined in Wittebort et al.; Vold, R. R. and Vold, R. L.; and Meints et al.[34,41,44] The ^{2}H NMR line shape $I(\omega,\tau_1,\tau_2,\Omega_{CL})$obtained by application of the quadrupolar echo pulse sequence (described in the section 2.2) to a polycrystalline sample is the Fourier transform of the time domain response $m(t)$:

$$I(\omega, \tau_1, \tau_2, \Omega_{CL}) = \mathrm{Re}\int m(t)e^{i\omega t}\mathrm{d}t \tag{2}$$

where the time domain response is

$$m(t) = \vec{1} \bullet Te^{\lambda(t+\tau_2)}T^{-1} \bullet T^*e^{\lambda(t+\tau_2)}(T^*)^{-1} \bullet \vec{m}_0 \tag{3}$$

and where λ and λ^* are eigenvalues of the matrices $A = i\omega + \pi$ and $A^* = -i\omega + \pi$, respectively. The matrix ω is diagonal with elements

$$\omega_i = \frac{3}{4}\frac{e^2qQ}{\hbar}\sum_{a=-2}^{+2} D^{(2)}_{0,a}(\Omega_i^{PC})D^{(2)}_{0,a'}(\Omega^{CL}) \tag{4}$$

where the solid angle Ω_i^{PC}relates the principal axis system (P) of the (uniaxial) electric field gradient tensor of the deuteron to the ith site along the reorientation trajectory of the C−D bond, which is defined relative to a molecular-fixed frame C. The second angle Ω^{CL} relates the molecular frame C to the laboratory frame L, and is averaged randomly in a polycrystalline sample.

To obtain a ^{2}H simulated line shape, the ω and π matrices must be determined. The ω matrix includes the set of angles $\{\Omega_i^{PC}\}$ that define the sequence of solid angles that orient the C−D bond in the C frame. The matrix ω may therefore be associated with the pathway or trajectory that the C−D bond follows. The matrix π includes information on the nature of the energy surface that the C−D encounters as it travels along the trajectory defined by ω as well as the diffusion coefficient that defines the rate at which a C−D bonds executes a mean displacement in the course of its travels along the trajectory. The structures of the two matrices ω and π used to obtain optimal fits to the experimental ^{2}H line shapes are separately discussed below.

2.3.2. Reorientational Trajectory. The simple models mentioned above have mostly treated the motion of the 5′ methylene group as an exchange between rotational isomers, where the rotation axis is collinear with the C4′−C5′ bond; however, the 4′ carbon is a component of the furanose ring whose displacements may couple to an extent to the 5′ methylene group. The reorientation of the C5′−D bond may not be described by a simple rotation about a single bond axis. To reflect coupling to the furanose ring motion, a lateral displacement of the 5′ carbon was incorporated into the dynamic model, where the trajectory of the C5′−D bond is described by a set of azimuthal/equatorial angles (θ_i,ϕ_i), where i labels the site along the trajectory. Typically 10 sites were used in a simulation to represent the 5′ methylene C−D bond trajectory. Discretizing the trajectory into more than 10 sites did not change the line shape inordinately.

From previous studies,[31,34] a global motion of the entire dodecamer about the helix axis is required to fit ^{2}H line shapes acquired at hydration levels greater than or equal to $W = 10$. The global motion is described by a six-site jump diffusion on a cone model. It was previously determined[42] that for hydration levels of $W = 10$ and above, the helical rate of rotation is 10^4 Hz. The half angle of the cone, which also describes the orientation of the local dynamic axis of the C5′−D bond with respect to the longitudinal helix axis, has previously been set to 20°, but for these studies of the more flexible phosphodiester backbone, it was varied from 20 to 60°.

2.3.3. Exchange Matrix. The set of angles that define the reorientational trajectory are used to calculate the Wigner rotation matrix elements in eq 4. To complete the propagation matrix A, the exchange matrix must be constructed according to eq 1. This requires a definition of the potential $U(\phi_i)$ and a value for the reorientation diffusion coefficient D so the correlation time τ can be determined. The simplest representation of the potential that the C5′−D5′/5″ bond might encounter during reorientation is an n-well potential function of the form

$$U(\phi_i) = \frac{U_0}{2}(1 - \cos n\phi_i) \tag{5}$$

where i labels the site along the discretized trajectory, U_0 is the barrier height, and n is the number of wells. In eq 5, $\phi_i = (2\pi/N)i$, where N is the number of discrete sites into which the trajectory is divided. For $N = 10$, $\phi_i = (\pi/5)i$. The simple expression in eq 5 can be modified to include wells with unequal depths, unequal barriers, etc. (Figure 4).[46] As a simple approximation to exchange between multiple wells, the exchange matrix is then defined by inserting eq 5 into eq 1. Assuming a given potential $U(\phi_i)$, line shapes are simulated as a function of U_0, D, and the angular displacement trajectory of the 5′ methylene group, described by the ranges of angles given in Table 3, given as a function of the lateral displacement of the 5′ carbon atom.

3. Results

To probe local mobility of the backbone in the d($G_5C_6G_7C_8$) site, deuterium line shapes and spin−lattice relaxation rates were obtained for the 5′/5″ deuterons of dG5, dC6, dG7, dC8, and 5-methyl-dC6. Experimental line shapes and line shape simulations are shown in Figure 5A and B. Motions ranging from ps−μs can be determined from the spin−lattice relaxation rates,

(46) Meints, G. A.; Karlsson, T.; Drobny, G. P. *J. Am. Chem. Soc.* **2001**, *123*, 10030–10038.

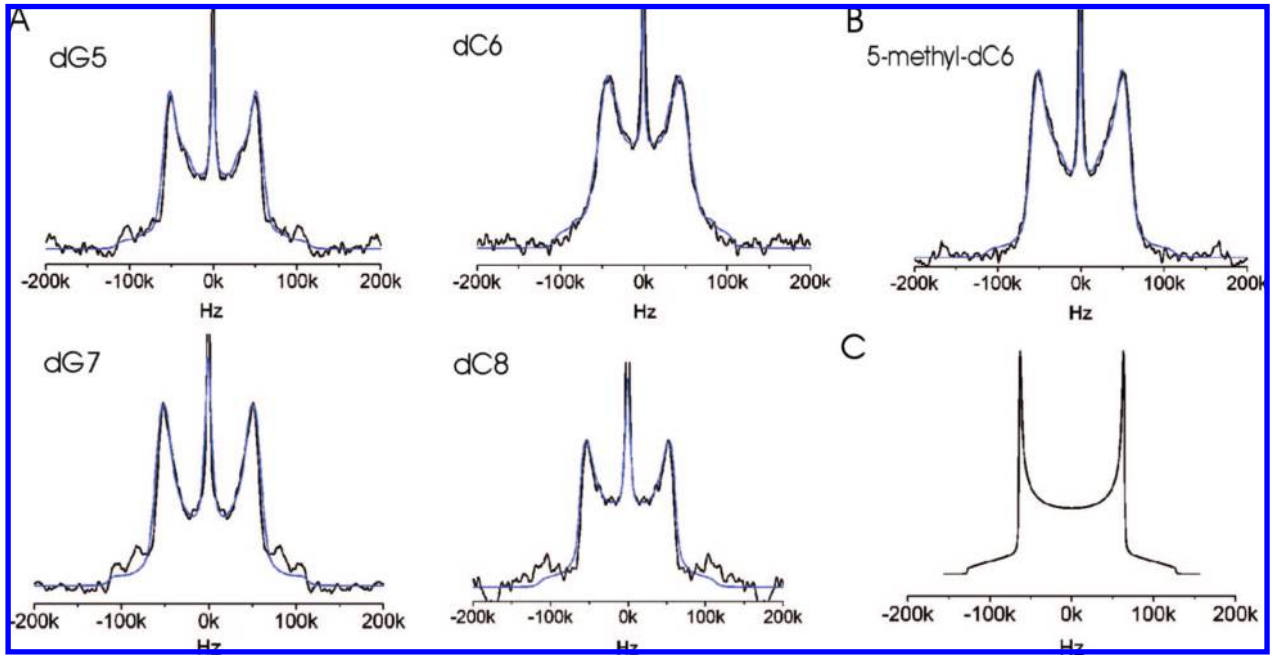

Figure 5. (A) Four deuterium line shapes (black) for each of the labeled sites in the nonmethylated DNA dodecamer with the simulation (blue) of each overlaid. Simulation parameters are described in Table 2. (B) Experimental solid-state deuterium line shape obtained for D5′/5″ in the backbone of methylated C6 (black) and simulated line shape (blue). (C) Spectrum of classical Pake doublet. The width between the horns is 3/4 of the quadrupolar coupling constant, which is 140−220 Hz for deuterium.

Table 1. Quantitative Values of Key Features of the Five Experimental Line shapes in Figure 5

label site	horn width (kHz)	QCC_{eff} (kHz)	Λ	center height (% of total height)	full width at half max. (kHz)
G5	102 ± 2	136 ± 2	0.78	47%	118 ± 2
C6	90 ± 2	120 ± 2	0.69	57%	114 ± 2
G7	104 ± 2	139 ± 2	0.79	38%	108 ± 2
C8	106 ± 2	141 ± 2	0.81	56%	121 ± 2
5mC6	105 ± 2	140 ± 2	0.80	46%	125 ± 2

Table 2. Spin-Lattice Relaxation Time for [5′/5″-^{2}H]-dG5 through dC8 from the DNA Sequence [d(GATA$G_5C_6G_7C_8$TATC)]$_2$

sample (from [d(GATA$\mathbf{G_5C_6G_7C_8}$TATC)]$_2$)	hydration (waters/nucleotide)	$\langle T_{1Z} \rangle$ (ms)
[5′/5″-^{2}H]-dG5	$W = 11.3 \pm 1$	68 ± 7
[5′/5″-^{2}H]-dC6	$W = 11.8 \pm 1$	46 ± 4
[5′/5″-^{2}H]-dG7	$W = 11.0 \pm 1$	53 ± 3
[5′/5″-^{2}H]-dC8	$W = 11.0 \pm 1$	51 ± 4
[5′/5″-^{2}H]-5-methyl-dC6	$W = 11.3 \pm 1$	71 ± 6

which are calculated from partially relaxed line shapes (Figure 6). Simulations can elucidate the detailed nature of local molecular motions including the direction and amplitude of reorientational motion.

Deuterium spin interactions are dominated by the modulation of the electric quadrupole moment with the surrounding electric field gradients and are not largely influenced by CSA or dipolar couplings. In contrast to relaxation studies of spin $^1/_2$ nuclei, where dynamic properties can only be compared from the relaxation of magnetically similar spins, the relative dynamics of deuterons can be obtained on a qualitative level and to a good approximation by straightforward comparison of relaxation and line shape data regardless of structural site. Knowledge of the electric field gradient (EFG) tensor is still critical for evaluation of relaxation and line shape data, but fortunately tensor variations are small for deuterons bonded to aliphatic carbons, allowing for direct comparisons between different sites.

3.1. Qualitative Analysis of the Line Shape and Partially Relaxed Line Shape Data. Static line shape experiments probe motions ranging from ns−ms time scale. Motions with rates occurring in this range produce "intermediately-averaged" line shapes, which differ from the classical Pake doublet (Figure 5C) most often by raising of the center of the line shape, narrowing of the overall line shape, and a loss of definition of the perpendicular edges, "the horns," of the type shown in Figures 5A and B with quantification of the line shape features in Table 1. Qualitatively, the extent of motion is manifested by the amount of deviation from the Pake doublet form.

The quadrupolar echo line shape of dG5 (Figure 5A) shows a narrowed classical Pake doublet with slightly broadened horns, a slightly raised center, while the inner edge of the horns becomes jagged; the dG7 line shape is quite similar and, of all the residues in the recognition site, deviates the least from the classical Pake doublet form, with only a slight rise in the center of the line shape and less narrowing of the overall line shape and broadening in the horns (Table 1). The dC6 and dC8 line shapes deviate substantially from the classic pake doublet form. Here, both the centers are markedly raised and the horns are broadened and beginning to lose definition. In addition, the dC6 line shape is significantly more narrowed that either the dG5 or dG7 (Table 1). The line shape results indicate the dC6 is significantly more mobile than the other sites on the ns−ms time scale, followed by dC8, and then dG5 and dG7.

The $\langle T_{1z} \rangle$ values (Table 2) also suggest that dC6 (46 ± 4 ms) is the most mobile site. Interestingly, both dG7 (53 ± 3 ms) and dC8 (51 ± 4 ms) have comparable spin−lattice relaxation times, (only slightly less than dC6) implying that they have the same degree of motion. Here, the $\langle T_{1z} \rangle$ value of dG5 (68 ± 7 ms) is significantly longer than the others indicating less mobility. These results are not contrary but highlight the differences in timescales that these two experiments probe. Whereas dC6 and dC8 appear to be able to exhibit motions over a large time scale (ps−ms), both dG5 and dG7 exhibit

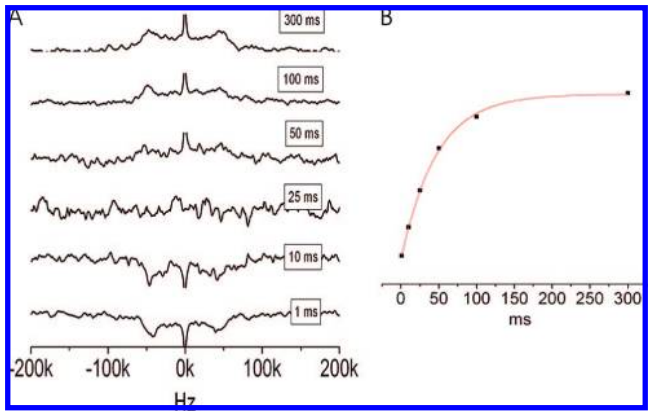

Figure 6. (A) Experimental inversion recovery line shapes of [5′/5″-D]-dC6 and (B) powder averaged $\langle T_{1z} \rangle$ exponential decay curve.

mobility over a smaller range of timescales; dG5 appears to exhibit motions slow motions (μs−ms) whereas dG7 experiences fast motions (ps−ns).

There is a significant change in the line shape of [5′/5″-D]-dC6 upon methylation (Figure 5A and B), as the horns expand and "unbend," approaching the classical Pake doublet line shape, indicating that this site becomes more rigid upon methylation. Additionally, the $\langle T_{1z} \rangle$ value increases (46 ± 4 to 71 ± 6 ms) from the unmethylated to methylated dC6. Though the extent of the dynamics of dC6 is not clear from the line shapes and relaxation data, what does remain clear is the dramatic loss of mobility associated with the methylation of dC6.

The backbone dynamics can also be discussed through an analysis of the quadrupolar coupling constant:

$$QCC = \frac{e^2qQ}{h} \tag{6}$$

The static QCC for the 5′/5″-methylene deuteron is $QCC_{\text{static}} = 175 \pm 1$ kHz.[42] For deuterium powder patterns that retain a Pake pattern, the amplitude reduction factor (ARF) Λ, can be used to assess motional averaging of the QCC. The ARF is defined as

$$\Lambda = \frac{QCC_{\text{eff}}}{QCC_{\text{static}}} = \frac{\left(\frac{e^2qQ}{h}\right)_{\text{eff}}}{\left(\frac{e^2qQ}{h}\right)_{\text{static}}} \tag{7}$$

and can be roughly equated to an order parameter. For dC6, the value of 120 ± 2 kHz for QCC_{eff} gives a value of Λ of 0.69. For 5-methyl-dC6, QCC_{eff} is 140 ± 2 kHz and Λ is 0.80, which is on the same order as the QCC_{eff} and Λ values for the nontarget bases in the recognition sequence (Table 1). This implies differential motional averaging in the methylated versus unmethylated DNAs, with motional averaging of the phosphodiester backbone being significantly diminished in the methylated DNA.

3.2. Quantitative Analysis. In earlier work,[31,42] the motion of the 5′ methylene group was portrayed as an exchange between the +sc, ap, and −sc rotational isomeric states, with a priori populations for the three states unequally weighted. Efforts to fit the ^{2}H solid-state line shapes in Figure 5A and B to that model failed to obtain close fits to the data; hence, for this study, other models were tested. As mentioned above, it was assumed that as a result of coupling to the furanose motion, the reorientational motion of the 5′ methylene C−D bonds are not simple rotations about the C4′−C5′ bond axes. A lateral displacement of the 5′ carbon results from coupling to the furanose motions and results in a reorientational trajectory that is a function of two angles $\{\theta_i,\phi_i\}$, the azimuthal and equatorial angles that orient the bond in the local molecular coordinate frame. In addition to the lateral motion, simulations indicate the root-mean-square amplitude of motion is considerably less than expected for an exchange between rotational isomers. Table 3 shows the average position along the reorientational trajectories for the C−D bonds of the 5′ methylene group and the maximum range in both θ and ϕ as a function of the lateral displacement of the 5′ carbon. Although the 5′ methylene group is randomly deuterated and different trajectories would be expected for the C5′−D5′ and C5′−D5″ bonds, bonding geometry makes only a single trajectory independent. The parameters describing the best-fit line shapes are shown in Table 4. The dG5 line shape was simulated best by a two-well periodic potential with unequal barriers of $2k_BT$ and $4.5k_BT$ with a lateral displacement of the C5′ of 0.3 Å and a jump rate of 10^8 Hz where the z_{local} is 50° above the plane of the helical rotation. The dG7 line shape was fit with a two-well potential with higher barriers of $4k_BT$ and $8k_BT$. The lateral displacement of the 5′ carbon and jump rate k were 0.32 Å and 10^8 Hz as before, and the orientation of z_{local} at this site was 40° above the plane of the helical rotation. The dC8 line shape was fit by a two-well potential with unequal barriers of $1k_BT$ and $3k_BT$, an amplitude of 0.32 Å, and a jump rate of 10^8 Hz with the orientation of z_{local} at this site of 30° above the plane of the helical rotation.

Table 3. Average Position and Maximum Displacement of the Trajectories of C5′−D5′/5″ for the C5′ Lateral Displacement Values Used in These Simulations

lateral displacement of C5′	average position (θ,ϕ)	max. range of θ	max. range of ϕ
0.30Å	(81.8,325.2)	16°	43°
0.32Å	(81.9,325.2)	17°	46°
0.37Å	(82.2,325.1)	20°	52°

Table 4. Values for U_0 along with Other Parameters Used to Fit Each of the 5 Simulated Line Shapes in Figure 5[a]

label site	U_0 ($0 \le \phi\pi$) (J)	U_0 ($\pi \le \phi < 2\pi$) (J)	amplitude (Å)	jump rate (Hz)	θ
G5	$2k_BT$	$4.5k_BT$	0.30	10^8	50
C6	$1.5k_BT$	$1.5k_BT$	0.37	10^9	60
G7	$4k_BT$	$8k_BT$	0.32	10^8	40
C8	$1k_BT$	$3k_BT$	0.32	10^8	30
5mC6	$2.5k_BT$	$4.5k_BT$	0.32	10^8	40

[a] The potential used for these simulations was $U(\phi_i) = U_0/2[1 - \cos(2\phi_i)]$.

The unmethylated dC6 line shape differed significantly from the nontarget sites and was best fit using a simple equal barrier two well-potential with barriers of $1.5k_BT$. Both the amplitude (0.37 Å) and jump rate (10^9 Hz) were larger than the other sites, and the z_{local} orientation was the largest (60°). This indicates that the dC6 5′/5″ deuterons are equally likely to be in the two most-favored conformations and that they are moving at a greater rate through a larger volume in space than the neighboring sites.

Upon methylation, the dC6 line shape is best modeled by parameters that are similar to the nontarget sites with a 5′ carbon displacement that is decreased to 0.32 Å and a slower jump rate (10^8 Hz). A two-well potential of unequal barriers of $2.5k_BT$ and $4.5k_BT$ (similar to dG5) and an orientation where z_{local} decreased to 40° describes the line shape the best. Each of these parameters support the conclusions drawn from the qualitative

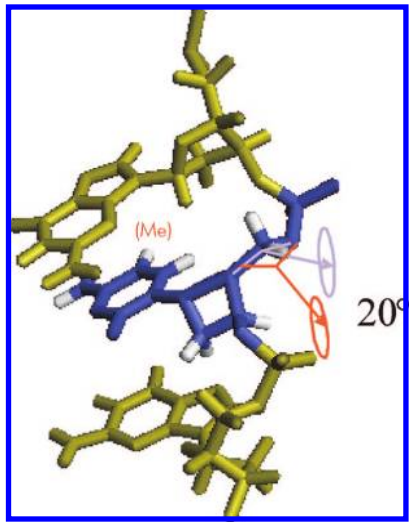

Figure 7. Impact of methylation on the orientation of the dynamic axis of the 5′ methylene group of nucleotide dC6.

analysis, namely, that there is a dramatic loss of conformational flexibility upon methylation of dC6, and demonstrate that upon methylation, the dynamics of the target nucleotide become similar to the nontarget sites in the recognition sequence.

4. Discussion

The process of DNA methylation and the impact that methylation exerts on [5′-GCGC-3′]$_2$ sequences has been extensively studied: structurally,[22,47–49] computationally,[18,20–22,25,50–52] and by dynamic spectroscopy.[14,31,32,53,54] Without doubt, the interactions between the phosphodiester backbone of the [5′-GCGC-3′]$_2$ recognition sequence and protein residues of the *Hha*I methyltransferase play an important role in extruding or "flipping" the cytosine base from its normal Watson−Crick based-paired position, a conformational change that optimally positions the cytosine base within the enzyme's catalytic pocket.

Given the evidence for the importance of the phosphodiester backbone in recognition and base flipping, how do the structurally redundant phosphodiester linkages of the DNA backbone manage to provide a template for specific recognition between the nucleic acid and the methyltransferase? There has been considerable investigation by MacKerell and co-workers[18] who suggest a form of "energetic recognition" between the DNA and the protein. Using computational methods, they demonstrated that the free-energy barriers to base flipping are significantly higher in noncognate DNA sequences than in the cognate sequence. On the basis of these computational studies, it is proposed that energetic recognition consists of a "web of protein-DNA interactions in short-lived, high energy states along the base flipping pathway."[18] Banavali and MacKerell go on to study the detailed mechanism of base flipping and find extensive changes in the torsion angles of the phosphodiester as a result of protein−DNA interactions.[25] Higher-energy and alternate low-energy regions of the (i.e., phosphodiester) dihedrals not usually populated in isolated DNA are observed in the authors' computations of base flipping.

Most of the experimental NMR evidence reported in this study corroborates these computations. Although the SSNMR dynamics observed at the phosphodiester backbone near the methylation target have yet to be compared to a large series of noncognate sequences, the line shapes and spin−lattice relaxation times observed for this particular segment in this [5′-GCGC-3′]$_2$ moiety have not been observed in other nucleotides in other DNA sequences. For example, in a DNA dodecamer containing the *Eco*RI recognition site, the deuterium relaxation times and line shapes observed in deuterated 5′ methylene groups at identical hydration states and temperature indicate a far more rigid phosphodiester backbone in A−T rich regions[42] and much less dynamic variation in the dihedral angles than occur near the methylation target site in the DNA dodecamer studied here. The dihedral angles of phosphodiester backbone in proximity to the methylation target site in the [5′-GCGC-3′]$_2$ moiety studies are much more dynamic on the ns−ms time scale. A qualitative analysis of both the line shapes and the relaxation data indicates that dC6 is the most mobile position in the recognition sequence.

The line shapes of the other sites in the recognition sequence and the methylated dC6 indicate some motion on the ms−ns time scale, whereas the $\langle T_{1z} \rangle$ values indicate that dG7 and dC8 experience additional dynamics on the ns−ps time scale. Although all four 5′ methylene groups studied here show diffusive motions between two low-energy conformations, the barriers to motion nearest the methylation target are equal and do not favor one conformation over the other. The root-mean-squared dynamic amplitude of the 5′ methylene group nearest the methylation target are also the largest observed. We conclude that this portion of the DNA's phosphodiester backbone is dynamically predisposed to structural distortions of the kind that must accompany base flipping, in particular changes in the γ torsion angles.

This study also shows that methylation exerts an impact on several aspects of the dynamics of the phosphodiester backbone near the methylation target site, including reduction of the amplitude of the dynamics and perturbation of the direction of the dynamics as indicated by a change in the orientation of the local dynamic axis of the 5′ methylene group relative to the helix axis. As in other restriction−modification systems, methylation of the target base in the *Hha*I binding site completely inhibits cleavage by the endonuclease. In addition, work by Klimasauskas et al. shows that methylation at the 5 carbon position on the target cytosine base also reduces 2−4 fold the binding affinity of the Mtase.[55] Therefore, the same chemical change that reduces methylase binding also perturbs the phosphodiester dynamics near the methylation target.

An interesting conclusion of the ^{2}H solid-state line shape study is that the dynamic axis frame of the 5′ methylene group nearest the methylation site has its z axis at about 60° relative

(47) Allan, B. W.; Reich, N. O.; Beechem, J. M. *Biochemistry* **1999**, *38*, 5308–5314.
(48) Vilkaitis, G.; Merkiene, E.; Serva, S.; Weinhold, E.; Klimasauskas, S. *J. Biol. Chem.* **2001**, *276*, 20924–20934.
(49) Lindstrom, J.; William, M.; Flynn, J.; Reich, N. O. *J. Biol. Chem.* **2000**, *275*, 4912–4919.
(50) Priyakumar, U. D.; MacKerell, A. D., Jr *J. Am. Chem. Soc.* **2006**, *128*, 678–679.
(51) Priyakumar, U. D.; MacKerell, A. D., Jr *Chem. Rev.* **2006**, *106*, 489–505.
(52) Huang, N.; MacKerell, A. D., Jr *J. Mol. Biol.* **2005**, *345*, 265–274.
(53) Neely, R. K.; Daujotyte, D.; Grazulis, S.; Magennis, S. W.; Dryden, D. T. F.; Klimasauskas, S.; Jones, A. C. *Nucleic Acids Res.* **2005**, *33*, 6953–6960.
(54) Miller, P. A.; Shajani, Z.; Meints, G. A.; Caplow, D.; Goobes, G.; Varani, G.; Drobny, G. P. *J. Am. Chem. Soc.* **2006**, *128*, 15970–15971.
(55) Klimasauskas, S.; Roberts, R. J. *Nucleic Acids Res.* **1995**, *23*, 1388–1395.

to the helix axis and differs from other 5′ methylene groups within the $[5'\text{-GCGC-}3']_2$ moiety, which are at much smaller angles to the helix axis. As a result the direction of reorientation of the 5′ methylene group of the C6 target nucleotide differs considerably from those of other 5′ methylene groups within the $[5'\text{-GCGC-}3']_2$ sequence. Upon methylation, the orientation of this frame changes by 20° and becomes similar to the other 5′ methylene groups of the $[5'\text{-GCGC-}3']_2$ moiety (Figure 7). This unique orientation of the 5′ methylene of dC6 may serve to better position this segment of the phosphodiester backbone for interacting with the methyltransferase. It is common in both solid-state and solution NMR to characterize the internal motions of biomolecules in terms of amplitudes (e.g., generalized order parameters) and correlation functions or rates. If the unique direction of the dC6's 5′ methylene reorientation better accommodates the initiation of base flipping, it is a unique instance in which the orientation of the dynamic axis frame contributes to function.

5. Conclusion

Here we have collected line shape data and measured $\langle T_{1z} \rangle$ for the methylene groups within the phosphodiester backbone of the DNA recognition site for the *Hha*I methyltransferase. A qualitative analysis of both the line shapes and the relaxation data indicates that dC6 is the most mobile position in the recognition sequence. Although both deoxycytidine residues display dynamic behavior within their furanose rings,[34] only the dC6 position has significant motional averaging in its backbone methylene moiety. This suggests that the dynamics observed at this position, which is the target site of the *Hha*I methyltransferase, might play some sort of role in the restriction−modification mechanism.

The local dynamics may play an important role in the initiation of base flipping, with the target site showing more local conformational flexibility than any other position within the binding site, which effectively lowers the barrier for conformational changes of the phosphodiester backbone necessary for cytosine base extrusion. Our simulations show that in addition to a decrease in the amplitude of the local motion, seen both in the furanose ring and the backbone, the angle between the z axis of the dynamic axis frame of the 5′ methylene group of dC6 and the helix axis decreases upon methylation, which may place the segment of the phosphodiester backbone nearest the methylation target in a position less optimal for interactions with the endonuclease.

Acknowledgment. We thank Professors Robert Vold, Gabriele Varani, J. Michael Schurr, and Bruce Robinson for helpful discussion in interpreting relaxation data. This research was supported by a grant from the NIH (RO1 EB003152) and a grant from the NSF (MCB-0642253).

JA801243D